Supplementary Information: Uniform, homogenous coatings of carbon nanohorns on arbitrary substrates from common solvents

*Landon Oakes[1,2], Andrew Westover[1,2], Masoud Mahjouri-Samani[3], Shahana Chatterjee[1], Alexander A. Puretzky[3], Christopher Rouleau[3], David B. Geohegan[3], and Cary L. Pint[1,2,]**

[1]Department of Mechanical Engineering, Vanderbilt University, Nashville, TN

[2]Interdisciplinary Materials Science Program, Vanderbilt University, Nashville, TN

[3]Center for Nanophase Materials Sciences and Materials Science Division, Oak Ridge National Laboratory, Oak Ridge, TN

1. Raman spectra and CNH/CNT dispersions

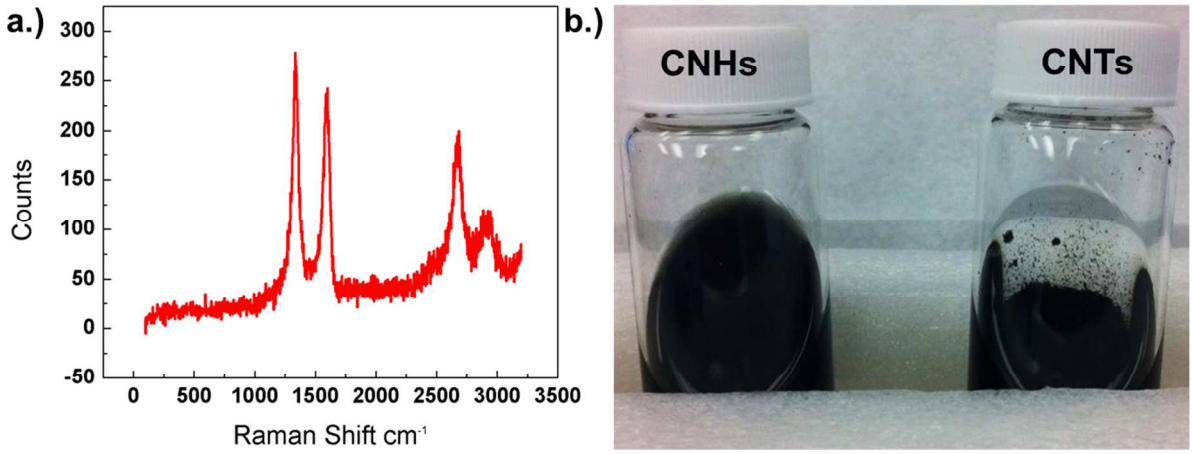

Figure S1. a.) Raman spectra from an electrophoretically deposited material of single-walled carbon nanohorns. Notable is the large D band emphasizing the large defect density of the nanohorns, and the G' mode that is comparable in height to the G mode that is representative of single and few-layer sheets that make up the nanohorns. b.) Dispersions of single-walled carbon nanohorns (left) and single-walled carbon nanotubes (right) in THF. The dramatic difference in the homogeneity of the dispersions is directly correlated to the defect density of the two materials. A high defect density allows for a greater degree of functionalization which allows for greater dispersion in solvents.

2. Zeta Potential Measurements

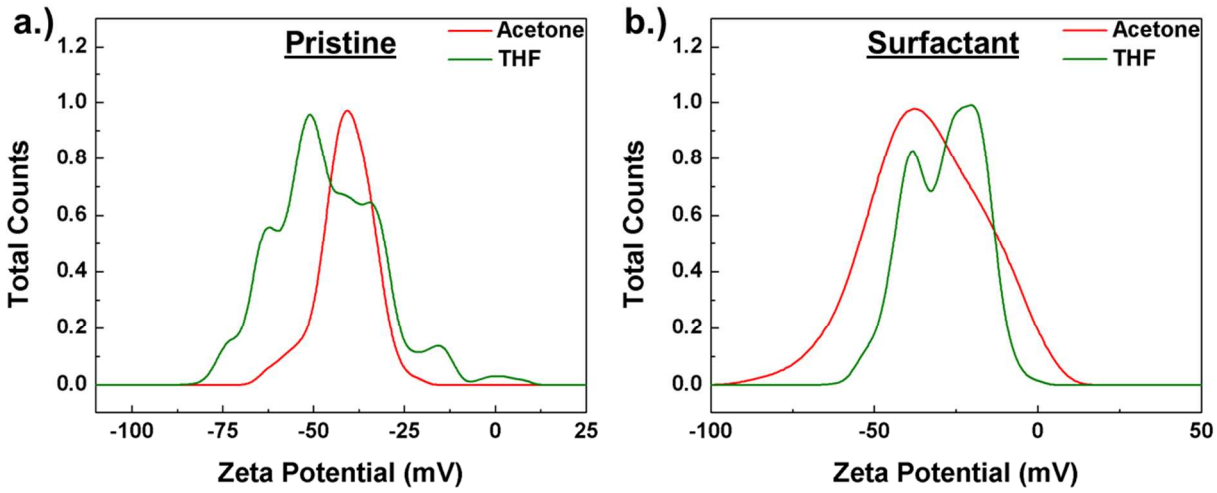

Figure S2. Zeta potential measurements of the solutions studied for dispersions of a.) pristine CNHs and b.) TOAB functionalized CNHs. Solutions with greater zeta potentials tend to deposit more rapidly than those with lower as the zeta potential is directly related to particle mobility within the solution.

3. Particle Size Distributions

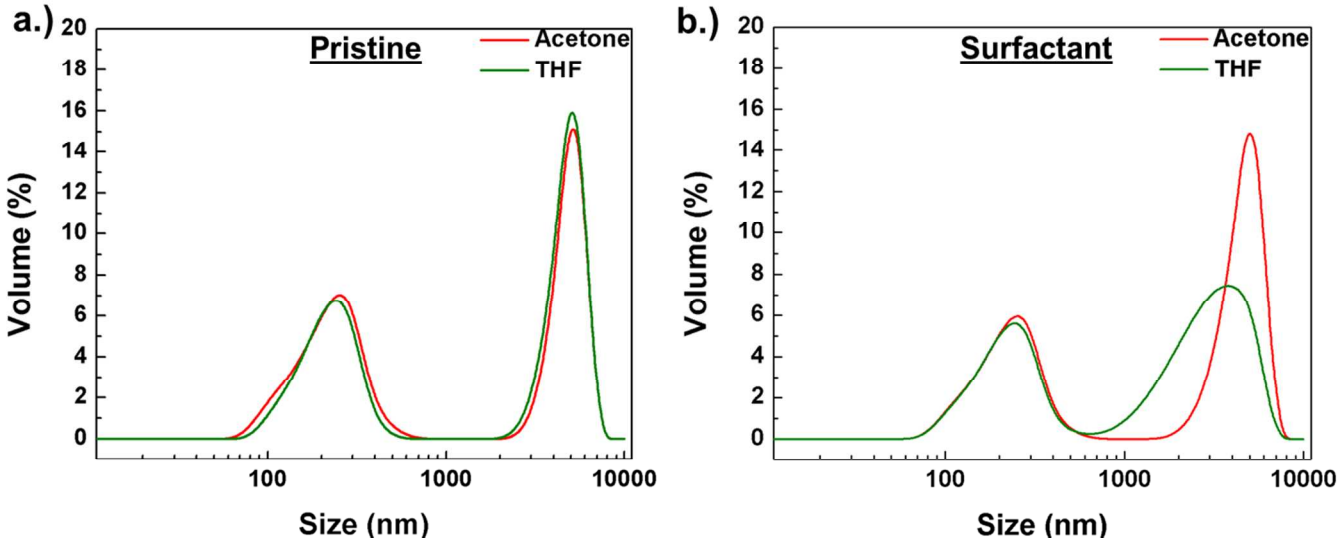

Figure S3. Particle size distributions of the solutions studied for dispersions of a.) Pristine CNHs and b.) TOAB functionalized CNHs. The particle distribution centered ~200nm is indicative of individual CNH clusters while the larger particles represents CNH aggregates. The use of a surfactant does not substantially influence the particle size distribution, but leads to a small increase in the peak size of the aggregates.

4. Depositions on Dielectric Surfaces

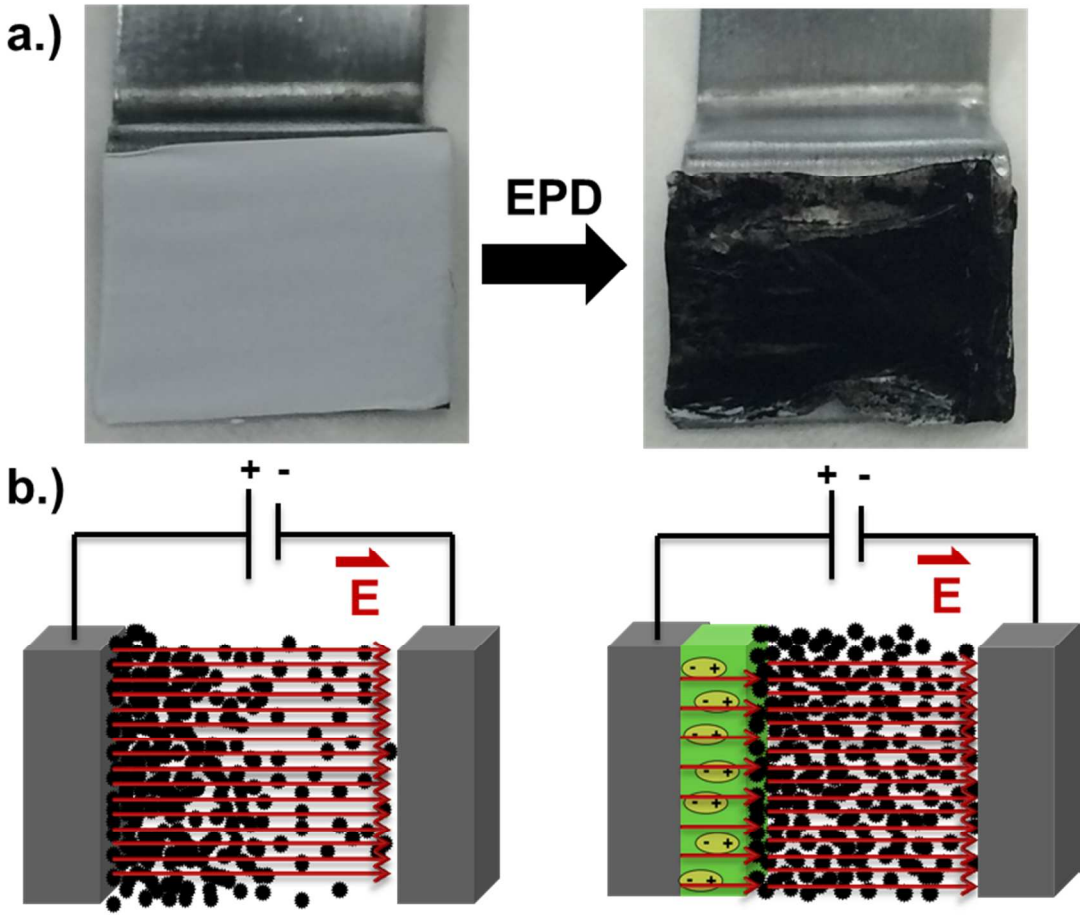

Figure S4. a.) Electrophoretic deposition of CNHs on teflon tape. Teflon tape is wrapped around a steel electrode and then submersed in the EPD solution facing the counterelectrode. b.) corresponding schematic for deposition on dielectric surfaces. The presence of an insulating material between the electrodes degrades the magnitude of both the electric field and surface charge on the substrate, however, deposition still occurs albeit at a much slower rate.

5. Current Deposition Profiles on Stainless Steel Substrates

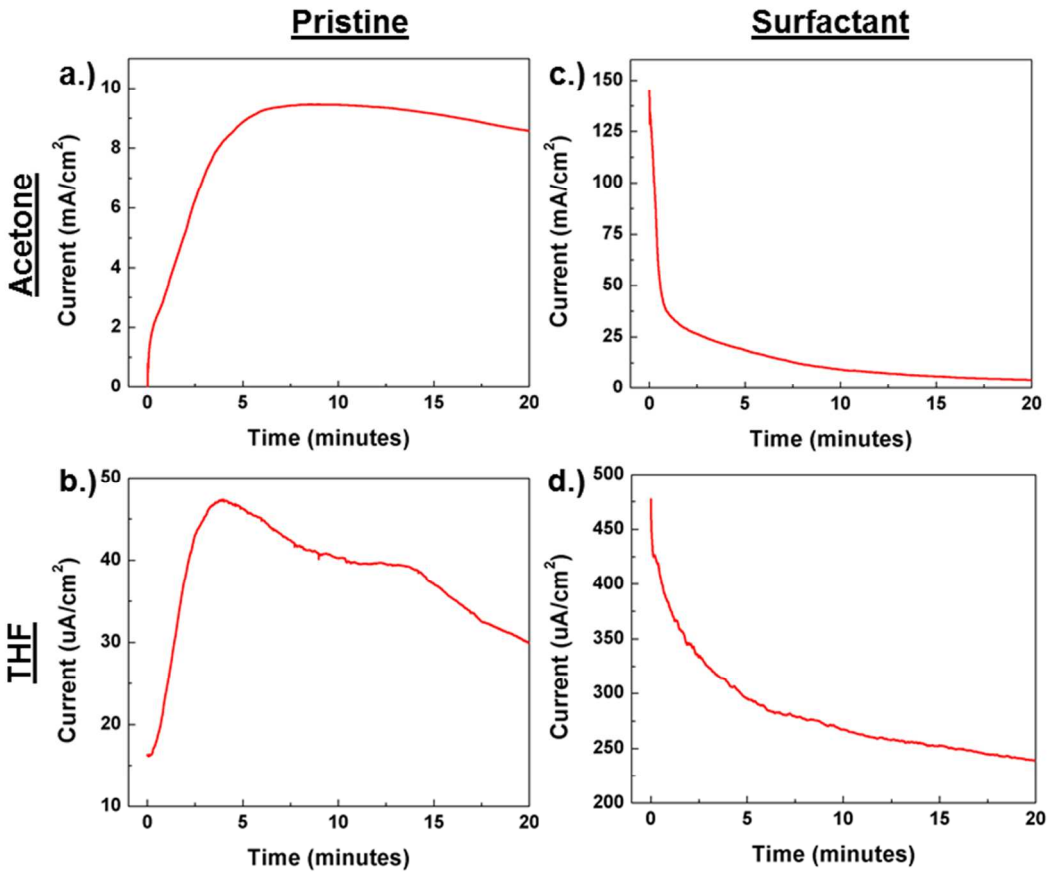

Figure S5. Current deposition profiles for the EPD of pristine CNHs dispersed in a.) Acetone and b.) THF. The steady rise in current is attributed to increasing concentrations of charged CNH particles near the surface of the electrode, after a dense coverage is formed the film begins to inhibit charge transfer and a decay in the magnitude of charge transfer is observed. Depositions with functionalized CNHs in c.) Acetone and d.) THF yield a different deposition profile reminiscent of the build-up of insulating layers of surfactant materials on the electrode surface.

6. Current deposition profiles from water and on dielectric surfaces

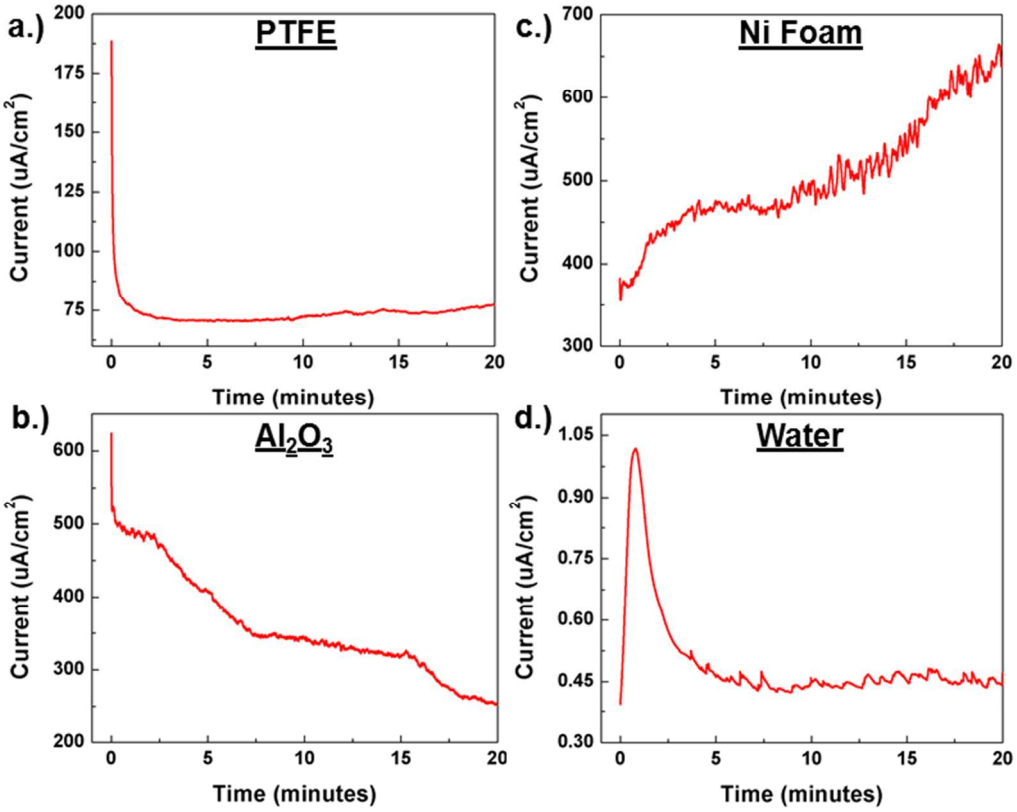

Figure S6. Current deposition profiles for the electrophoretic deposition of pristine CNHs onto a.), b.) dielectric surfaces. The initial rapid drop in current is likely due to the polarization of the dielectric medium; the subsequent rise is attributed to an increasing CNH concentration near the electrode's surface. The deposition profile on c.) nickel foam exhibits a constant increase as the immense surface area of this electrode relative to the other substrates studied requires a much greater time to achieve a coating dense enough to significantly inhibit charge transfer. d.) Deposition onto conducting steel electrodes from TOAB functionalized CNHs dispersed in water shows an initial rapid increase in current due to the presence of conducting ions inherit to water (H+ and OH-), however, the presence of surfactant within solution leads to behavior similar to that found in organic solvents. The lower applied voltage (1.1V to avoid electrolysis) broadens the timescale over which this phenomena occurs.

7. SEM observation of CNH infiltration into Nickel Foam

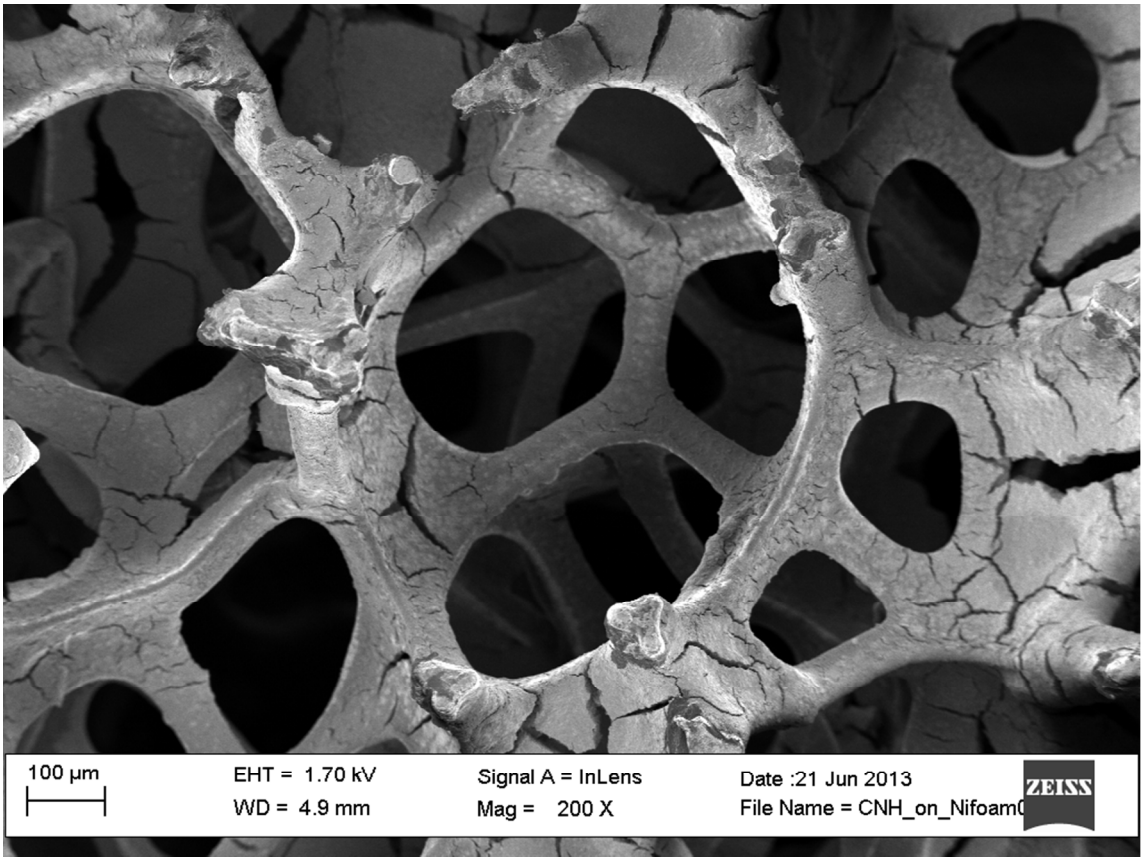

Figure S7. SEM image of single-walled CNH films deposited onto a 3-D Ni foam. Of particular note in this image are the cracks in the deposited CNH film coating that can be visibly observed deep inside of the Ni foam material, emphasizing the presence of a CNH coating that uniformly extends into the 3-D structure of the Ni foam.

8. Gas Sensing Schematic

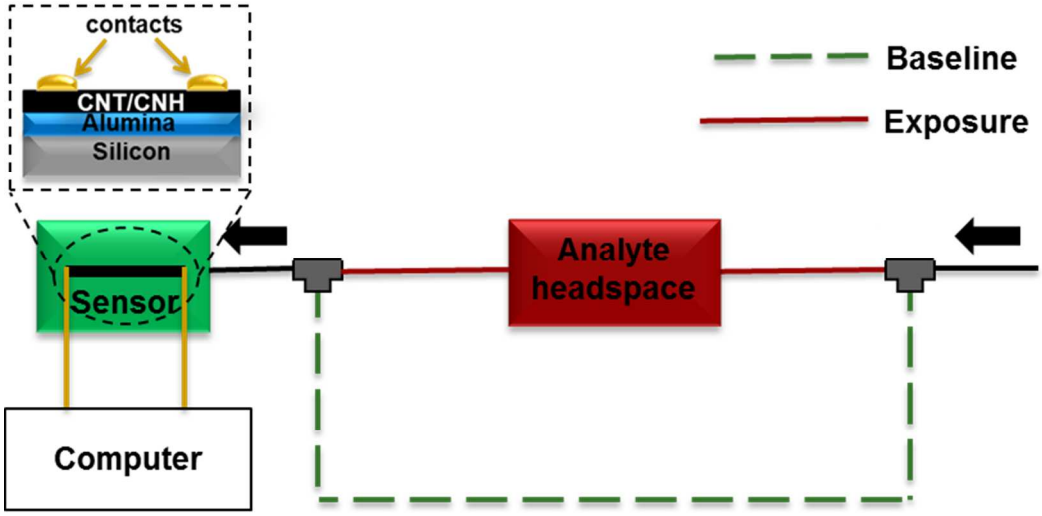

Figure S8. Gas sensing schematic for the gas sensors studied. During acquisition of the baseline, a pure Argon flow is exposed to the sensor through a path indicated by the green dotted line. During exposure, flow is redirected to a headspace filled with the analyte vapor by the path indicated by the red solid line.

9. Additional images of CNH coated materials

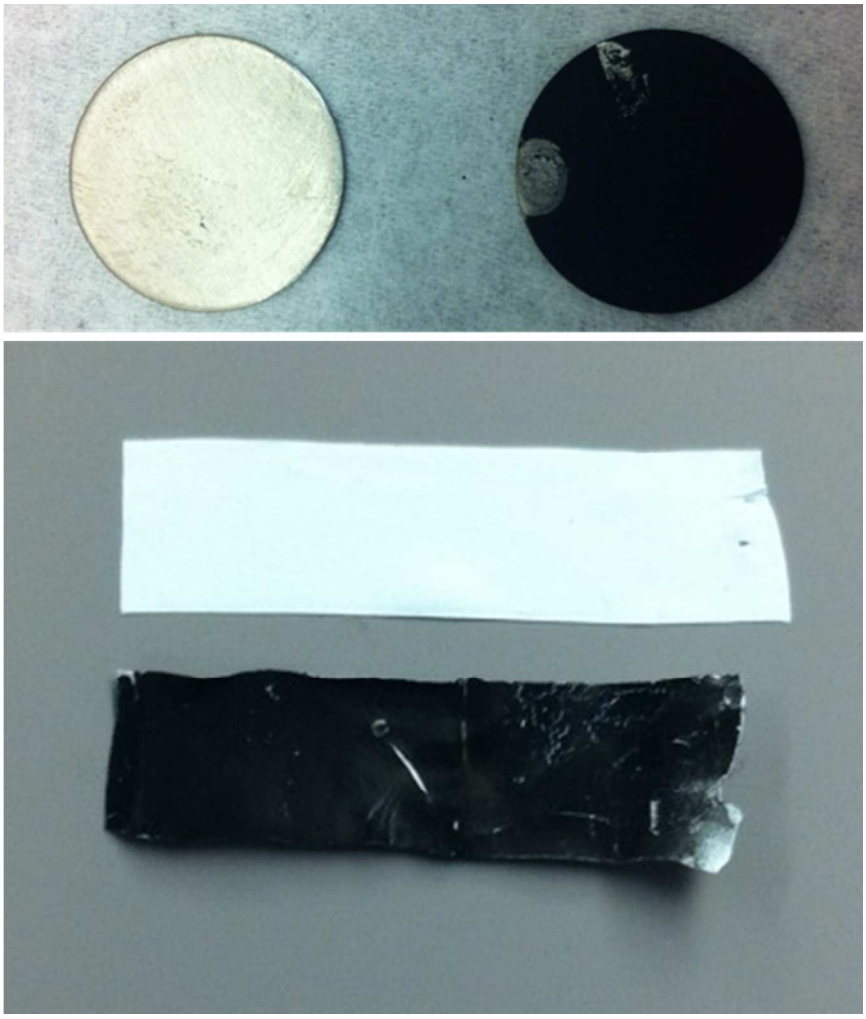

Figure S9. Photographs of carbon nanohorn films deposited onto (top) stainless steel discs that are utilized in battery coin cells, and (bottom) a piece of PTFE tape. Notable is the uniformity of coating on both substrates, and the flexible nature of the coating on the PTFE tape.